Provided for non-commercial research and education use.
Not for reproduction, distribution or commercial use.

This article appeared in a journal published by Elsevier. The attached copy is furnished to the author for internal non-commercial research and education use, including for instruction at the authors institution and sharing with colleagues.

Other uses, including reproduction and distribution, or selling or licensing copies, or posting to personal, institutional or third party websites are prohibited.

In most cases authors are permitted to post their version of the article (e.g. in Word or Tex form) to their personal website or institutional repository. Authors requiring further information regarding Elsevier's archiving and manuscript policies are encouraged to visit:

http://www.elsevier.com/copyright

Author's personal copy

Journal of Alloys and Compounds 472 (2009) 55–58

Contents lists available at ScienceDirect

Journal of Alloys and Compounds

journal homepage: www.elsevier.com/locate/jallcom

The improved electrochemical performance of SnSb-based alloy anode materials for Li-ion batteries

Fei Wang*, Mingshu Zhao, Xiaoping Song

Department of Materials Physics and Chemistry, School of Science, Xi'an Jiaotong University, Xi'an 710049, PR China

ARTICLE INFO

Article history:
Received 14 February 2008
Received in revised form 18 April 2008
Accepted 22 April 2008
Available online 6 June 2008

Keywords:
Lithium-ion battery
Anode
Nano-sized
SnSb alloy
Cycling performance

ABSTRACT

Nano-sized SnSb alloy anodes were prepared by reductive co-precipitation method combining with the aging treatment in water bath at 80 °C. The microstructure, morphology and electrochemical properties of synthesized SnSb alloy powders were evaluated by X-ray diffraction (XRD), field-emission scanning electron microscopy (FE-SEM) and galvanostatical cycling tests. The results indicated that the cycling performance of SnSb alloy anodes could be improved through reducing particle size. However, the capacity decline was still apparent in every cycle due to the poor reversible process of high voltage reaction. When the cut-off potential was limited between 0.02 and 0.9 V, the volume and structure changes are alleviated effectively and the excellent cycling performance was obtained within 20 cycles.

© 2008 Elsevier B.V. All rights reserved.

1. Introduction

Although carbonaceous materials, especially graphite carbons, are widely used as negative electrode materials in commercial rechargeable lithium batteries, the novel negative electrode materials with higher levels of safety and higher specific capacity than those offered by graphite are still desirable due to the increasing demand of higher performance batteries. Throughout the search for alternatives of carbonaceous materials, much efforts have been devoted to the use of Li alloys, such as Al, Sn, Sb, Si, etc., which can offer much higher specific capacity than that of traditional carbonaceous materials. However, metallic macro-materials undergo severe structural and volume changes during the lithiation/delithiation process compared with carbonaceous materials. This greatly limits the mechanical stability and the cycle life of the electrode [1–3].

To overcome the problem of reactant expansion, the basic method is the use of composite negative electrodes, which utilizes a 'buffer matrix' to compensate for the expansion of the reactants and thus, preserve the electrical pathway [4,5]. The representative materials include amorphous tin composite oxides (ATCO) [6], Sn–Fe–C [7–9] and other intermetallic alloys which show a strong structural relationship between the parent binary electrode and its lithiated product [10–14], etc. Substituting bulk materials by their nanoscale counterparts is another way to improve the cyclability of alloy anodes [4]. Firstly, the reducing of host size is an effective way to decrease the absolute volume changes and improve the mechanical stability [2,3]. Secondly, the large surface area and short diffusion paths in nanoscale materials are beneficial for electrode kinetics. Thirdly, nanoscale materials can enhance the reaction ability towards lithium and improve the electrochemical reversibility by suppressing the phase transformations [15–18].

In this work, we choose SnSb alloy anode prepared by reductive co-precipitation method to study the influence of particle size and cut-off potential to the electrochemical performance. SnSb-based alloy anodes have numerous merits, such as high theoretical Li storage capacity, strong structural relationship between the parent binary intermetallic phase and its lithiated product [13,14], cheap and environmental friendly, etc. In order to improve the morphology and electrochemical property of the alloy anode materials prepared by reductive co-precipitation, we treated with the freshly precipitated alloy particles by aging in constant temperature water bath at 80 °C. Our work shows that the aging treatment is a simple and efficient method to obtain comparative uniform phase components, integrated particles and good electrochemical performance [19].

2. Experimental

The alloy powders were synthesized by reductive co-precipitation of metal chlorides from aqueous solution with $NaBH_4$. To synthesize SnSb alloy powders, two

* Corresponding author at: Department of Materials Physics and Chemistry, School of Science, Xi'an Jiaotong University, Number 28, Xianning West Road, Xi'an, Shaanxi 710049, PR China. Tel.: +86 29 82675055; fax: +86 29 82667872.
E-mail address: feiwang@mail.xjtu.edu.cn (F. Wang).

0925-8388/$ – see front matter © 2008 Elsevier B.V. All rights reserved.
doi:10.1016/j.jallcom.2008.04.075

Author's personal copy

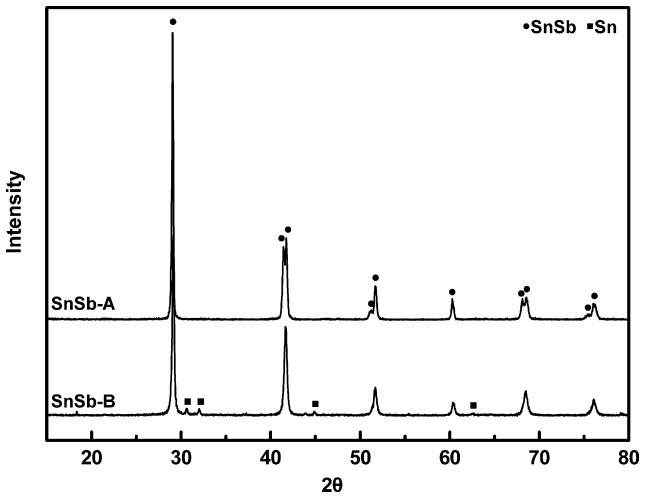

Fig. 1. XRD patterns of different SnSb alloy powders prepared by reductive co-precipitation method.

solutions were used. Solution A formed by 0.01 mol $SnCl_2{\cdot}2H_2O$, 0.01 mol $SbCl_3$ and 0.035 mol $C_6H_5Na_3O_7{\cdot}2H_2O$, which were mixed together and dissolved in 100 ml distilled water to form a 0.1 M solution of Sn^{2+}. Solution B is the 0.2 M alkaline $NaBH_4$ aqueous solution (pH > 12). Two reaction modes were used, namely solution B was added drop-wise into solution A under strong magnetic stirring at room temperature or solution A was added into solution B according to the same method. The superfluous $NaBH_4$ solution was used to ensure the complete reduction of the metal ions. The product synthesized by different reaction modes named SnSb-A and SnSb-B. After co-precipitation, all alloy powders in aqueous solution were aged in water bath with a constant temperature of 80 °C for 5 h. Finally, the solution was filtered and the product was washed thoroughly using distilled water and acetone. The black product was dried at 105 °C for 10 h under vacuum.

The crystal structure of alloy anode materials was detected by Shimadzu-7000 type X-ray Diffraction (XRD) with Cu Kα radiation. The morphology and particle size of alloy powders were observed by JSM-6700 field-emission scanning electron microscope (FE-SEM).

Electrochemical experiments were carried out in two-electrode Swagelok cells which were composed of a metallic lithium foil as counter electrode, 1 M LiPF6 in ethylene carbonate (EC)–diethyl carbonate (DEC) (1:1, v/v) as electrolyte, Celegard 2400 as separator and nano-sized alloy as the working electrode. The working electrodes were prepared by pasting slurry onto a copper foil substrate. The slurry consisted of 80 wt% alloy powder, 10 wt% acetylene black and 10 wt% polyvinylidene fluoride (PVDF) dissolved in NMP. Then the electrodes were dried in vacuum oven at 110 °C for 12 h prior to use. Testing cells were assembled in the argon-filled glove box and were cycled on the Arbin BT2000 battery tester at a constant current density of 0.1 mA cm^{-2}.

3. Results and discussion

The XRD patterns of two SnSb alloys prepared by reductive co-precipitation method are shown in Fig. 1. The 10 peaks in SnSb-A completely correspond with the rhombohedral phase of SnSb (β-SnSb). In SnSb-B, a small amount of ductile Sn can be found in addition to β-SnSb. Furthermore, the sharper XRD peaks indicate higher crystallinity and relatively larger crystallite size. Using Scherrer equation, the mean crystallite sizes of SnSb-A and SnSb-B can be estimated as 55 and 39 nm, respectively.

The reactants were same and all metal ions were ensured to be completely reduced, so there are small differences in composition of two SnSb alloys, while the differences in morphology shown in FE-SEM images (Fig. 2) are remarkable. From Fig. 2(a), it can be seen clearly that the primary particles of SnSb-A sample can hardly be identified, which aggregate to larger secondary agglomerates about 200 nm. The secondary particles are further connected with each other and exhibit loose morphology [2,20]. Unlike SnSb-A, the smaller primary particles of SnSb-B, which are close to their crystallite size, do not show severe aggregation to form larger secondary agglomerates but connect with

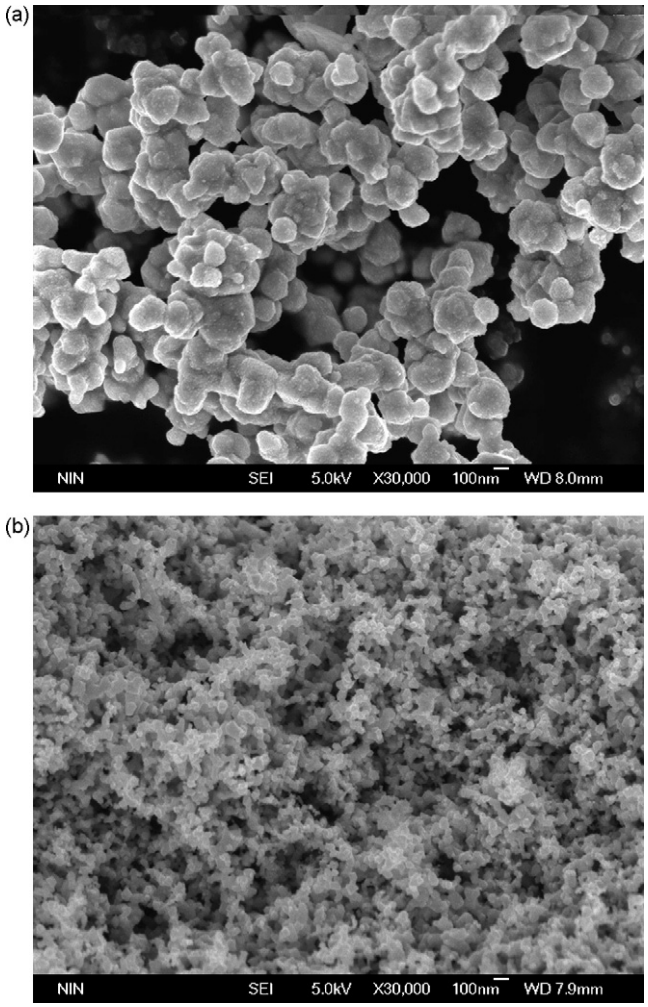

Fig. 2. FE-SEM images of different SnSb alloy powders prepared by reductive co-precipitation method: (a) SnSb-A and (b) SnSb-B.

each other to form loose morphology directly. The difference of two SnSb alloys in aggregation morphology should be controlled by dynamics. When the mixed solution (solution A) is added drop-wise to alkaline $NaBH_4$ solution (solution B), the diffusion and growth of initial nucleus are restrained by the low concentration of Sn^{2+} and Sb^{2+}. So smaller particles and lower aggregation appear in SnSb-B sample. The remarkable difference in morphology must influence the electrochemical performance significantly.

Fig. 3 compares the cycling performance of two SnSb alloy electrodes cycled between 0.02 and 1.5 V. It can be seen clearly that SnSb-B sample has superior cyclability than SnSb-A except the first cycle and the reversible capacities of SnSb-B reach 540 mAh g^{-1} after 20 cycles. Commonly, smaller particles have fewer tendencies to subdivide during cycling due to smaller absolute volume change and mechanical stress, which are favorable to enhance the morphological stability of particles and thus, improve the cycling performance. As shown in Fig. 4, the original particles of SnSb-A become larger and obviously tend to pulverize after 8 cycles, whereas the SnSb-B particles after 8 cycles have tendency to aggregation. Li et al. [21,22] said that when the particle size of active alloy materials is less than 100 nm, the aggregation caused by electrochemical alloy reaction with lithium generally occurs.

Moreover, the electrochemical performance of first cycle is also influenced by the morphology of two SnSb alloys. The voltage ver-

Author's personal copy

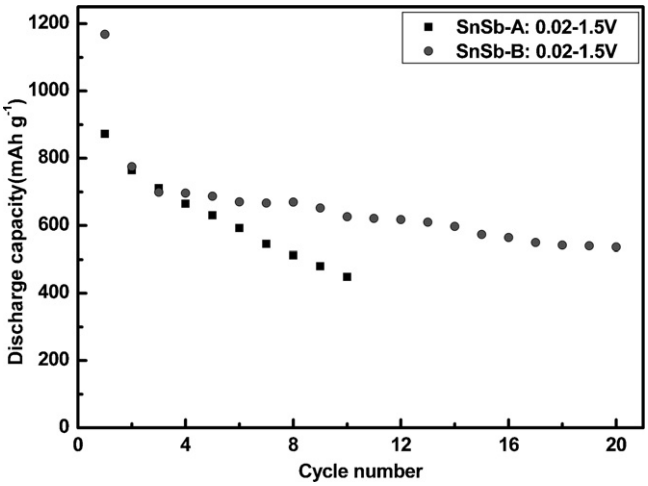

Fig. 3. Cycling performances of different SnSb alloy electrodes cycled between 0.02 and 1.5 V.

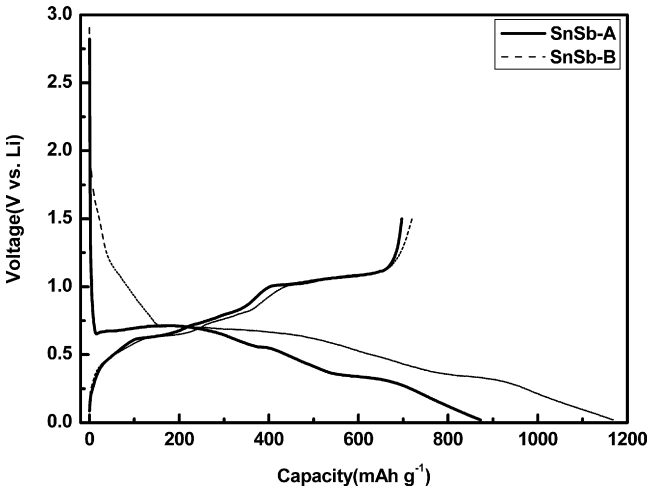

Fig. 5. Initial voltage profiles of different SnSb alloy electrodes.

sus specific capacity curves measured in the first cycle of two SnSb alloy electrodes are shown in Fig. 5. The main difference in two curves is the discharge curve above 0.75 V, which corresponds to some irreversible reactions such as the decomposition of electrolyte, the formation of solid electrolyte interphase (SEI) film and the reduction of oxide impurity. These irreversible reactions mainly lie on the specific surface area and surface oxide of alloy powders. SnSb-B sample has smaller particles and thus, has more specific surface area and surface oxide, which consequentially results in more initial irreversible capacities.

Although the cycling performance of SnSb-B sample has been improved remarkably by reducing the particle size, the capacity declining is still obvious in each cycle. Because the reducing of particle size cannot eliminate the influence of volume change and cannot effectively alleviate the influence of structure change, especially for SnSb alloy, in which two elements are electrochemically actives. As shown in Fig. 6, the capacities under 0.8 V have little changes after the first cycle, whereas the capacities above 0.8 V decline obviously along with the cycling. Lithium reacts with SnSb at approximate 0.8 V to form Li_3Sb and metallic Sn [23], which can be viewed simplistically as lithium insertion into, and tin displacement from, a Sb host structure [14]. This reaction is reversible [24], but it is dependent on the availability of extruded Sn atoms at the surface of Li_3Sb particles. Along with the discharging, the extruded Sn reacts to Li at lower potentials to yield Li_xSn ($0 < x < 4.4$). These low voltage reactions increase the electrode capacity, but also result in further volume and structure changes and a loss of interparticle contact between Li_3Sb and Sn compo-

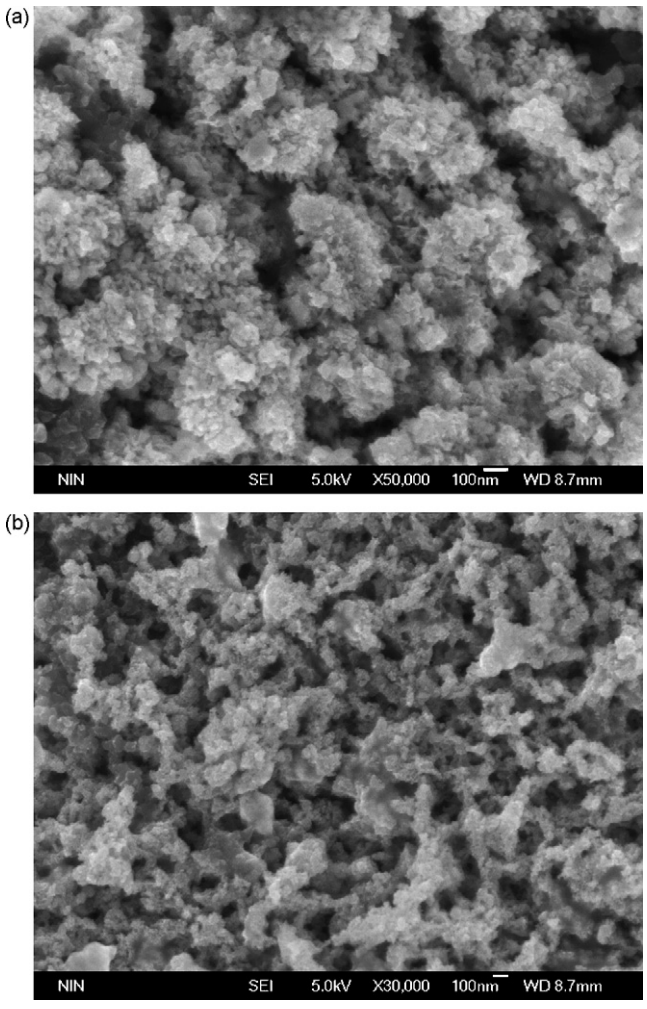

Fig. 4. FE-SEM images of different SnSb alloy electrodes after 8 cycles: (a) SnSb-A and (b) SnSb-B.

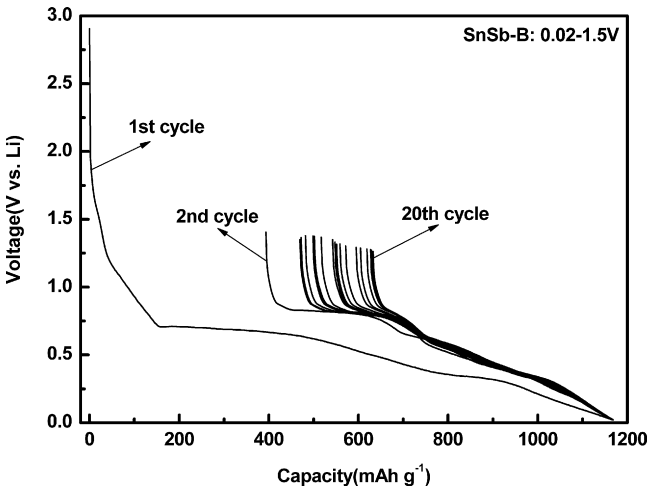

Fig. 6. Discharging voltage profiles of SnSb-B alloy electrode cycled between 0.02 and 1.5 V.

Author's personal copy

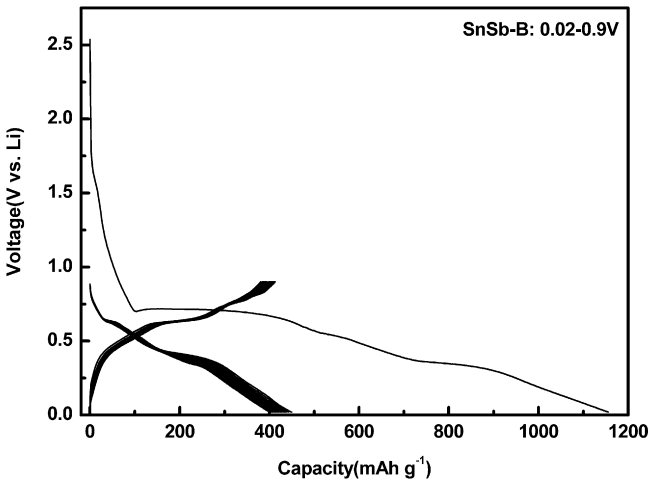

Fig. 7. Voltage profiles of SnSb-B alloy electrode cycled between 0.02 and 0.9 V.

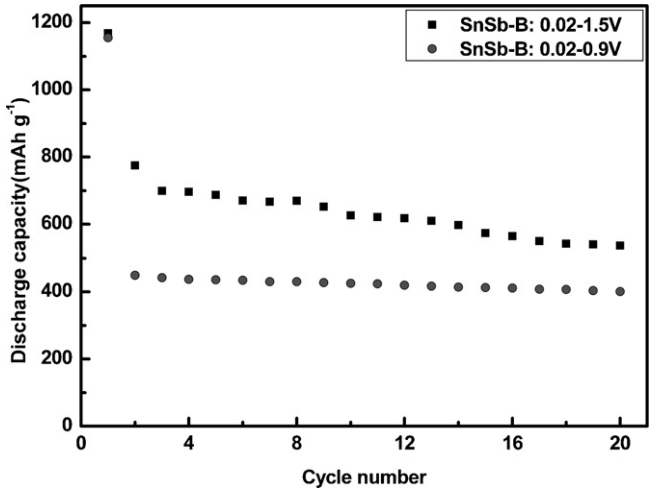

Fig. 8. Cycling performances of SnSb-B alloy electrode cycled in different cut-off potential.

nents, which compromise the reversibility of the reaction in high voltage between Li_3Sb and SnSb [25]. This poor reversible process leads to the declining of high voltage plateaus and cannot be avoided completely when cycled between 0.02 and 1.5 V in SnSb alloy. However, when the cut-off potential is limited between 0.02 and 0.9 V, the reaction between Li_3Sb and SnSb is prohibited and the Li_3Sb can be acted as an inert phase in whole reaction process. So, the volume and structure changes are alleviated effectively and the excellent cycling performance with the reversible capacities above 400 mAh g^{-1} is obtained within 20 cycles, as shown in Figs. 7 and 8.

4. Conclusions

In this work we have extended the investigation of SnSb alloy anodes prepared by reductive co-precipitation method. It showed that reducing particle size of SnSb alloy anodes could enhance morphological stability and thus, improved the cycling performance. However, the capacity declining was still evident in every cycle, which caused by the poor reversible process of high voltage reaction between Li_3Sb and SnSb. When we limited the cut-off potential between 0.02 and 0.9 V, the volume and structure changes are alleviated effectively and the excellent cycling performance with reversible capacities above 400 mAh g^{-1} was obtained within 20 cycles.

Acknowledgement

The authors would like to acknowledge Introduction of Talents Fund of Xi'an Jiaotong University (Grant No. 090071181) for providing financial support to this work.

References

[1] J. Yang, M. Winter, Solid State Ionics 90 (1996) 281.
[2] H. Li, X.J. Huang, L.Q. Chen, Z.G. Wu, Y. Liang, Electrochem. Solid State Lett. 2 (1999) 547.
[3] M. Winter, J.O. Besenhard, Electrochim. Acta 45 (1999) 31.
[4] J.-M. Tarascon, M. Armand, Nature 414 (2001) 359.
[5] A. Anani, S. Crouch-Baker, R.A. Huggins, J. Electrochem. Soc. 134 (1987) 3098.
[6] Y. Idota, T. Kubota, A. Matsufuji, Y. Maekawa, T. Miyasaka, Science 276 (1997) 1395.
[7] O. Mao, R.A. Dunlap, J.R. Dahn, J. Electrochem. Soc. 146 (1999) 405.
[8] O. Mao, J.R. Dahn, J. Electrochem. Soc. 146 (1999) 413.
[9] O. Mao, J.R. Dahn, J. Electrochem. Soc. 146 (1999) 423.
[10] M.M. Thackeray, J.T. Vaughey, A.J. Kahaian, K.D. Kepler, R. Benedek, Electrochem. Commun. 1 (1999) 111.
[11] J.T. Vaughey, J. O'Hara, M.M. Thackeray, Electrochem. Solid State Lett. 3 (2000) 13.
[12] L.M.L. Fransson, J.T. Vaughey, R. Benedek, K. Edstrom, J.O. Thomas, M.M. Thackeray, Electrochem. Commun. 3 (2001) 317.
[13] R. Benedek, M.M. Thacheray, J. Power Sources 110 (2002) 406.
[14] M.M. Thacheray, J.T. Vaughey, C.S. Johnson, A.J. Kropf, R. Benedek, L.M.L. Fransson, K. Edstrom, J. Power Sources 113 (2003) 124.
[15] D. Sun, C.W. Kwon, G. Baure, E. Richman, J. Maclean, B. Dunn, S.H. Tolbert, Adv. Funct. Mater. 14 (2004) 1197.
[16] P. Poizot, S. Laruelle, S. Grugeon, L. Dupont, J.-M. Tarascon, Nature 407 (2000) 496.
[17] P. Poizot, S. Laruelle, S. Grugeon, L. Dupont, J.-M. Tarascon, J. Power Sources 97–98 (2001) 235.
[18] D. Larcher, C. Masquelier, D. Bonnin, Y. Chabre, V. Masson, J.-B. Leriche, J.-M. Tarascon, J. Electrochem. Soc. 150 (2003) A133.
[19] F. wang, M.S. Zhao, X.P. Song, J. Alloys Compd. 439 (2007) 249.
[20] A. Trifonova, M. Wachtler, M.R. Wagner, H. Schroettner, Ch. Mitterbauer, F. Hofer, K.C. Möller, M. Winter, J.O. Besenhard, Solid State Ionics 168 (2004) 51.
[21] H. Li, X.J. Huang, L.Q. Chen, G.W. Zhou, Z. Zhang, D.P. Yu, Y.J. Mo, N. Pei, Solid State Ionics 135 (2000) 181.
[22] H. Li, L.H. Shi, W. Lu, X.J. Huang, L.Q. Chen, J. Electrochem. Soc. 148 (2001) A915.
[23] I.A. Courtney, J.R. Dahn, J. Electrochem. Soc. 144 (1997) 2045.
[24] J. Yang, Y. Takeda, N. Imanishi, J.Y. Xie, O. Yamamoto, Solid State Ionics 133 (2000) 189.
[25] I. Rom, M. Wachtler, I. Papst, M. Schmied, J.O. Besenhard, F. Hofer, M. Winter, Solid State Ionics 143 (2001) 329.